Available online at www.sciencedirect.com

SCIENCE DIRECT

Remote Sensing of Environment 95 (2005) 248–263

Remote Sensing of Environment

www.elsevier.com/locate/rse

Spectral mixture analysis for subpixel vegetation fractions in the urban environment: How to incorporate endmember variability?

Conghe Song*

Department of Geography, CB# 3220, 205 Saunders Hall, University of North Carolina at Chapel Hill, Chapel Hill, NC 27599, USA

Received 9 December 2003; received in revised form 4 January 2005; accepted 8 January 2005

Abstract

In the urban environment both quality of life and surface biophysical processes are closely related to the presence of vegetation. Spectral mixture analysis (SMA) has been frequently used to derive subpixel vegetation information from remotely sensed imagery in urban areas, where the underlying landscapes are assumed to be composed of a few fundamental components, called endmembers. A critical step in SMA is to identify the endmembers and their corresponding spectral signatures. A common practice in SMA assumes a constant spectral signature for each endmember. In fact, the spectral signatures of endmembers may vary from pixel to pixel due to changes in biophysical (e.g. leaves, stems and bark) and biochemical (e.g. chlorophyll content) composition. This study developed a Bayesian Spectral Mixture Analysis (BSMA) model to understand the impact of endmember variability on the derivation of subpixel vegetation fractions in an urban environment. BSMA incorporates endmember spectral variability in the unmixing process based on Bayes Theorem. In traditional SMA, each endmember is represented by a constant signature, while BSMA uses the endmember signature probability distribution in the analysis. BSMA has the advantage of maximally capturing the spectral variability of an image with the least number of endmembers. In this study, the BSMA model is first applied to simulated images, and then to Ikonos and Landsat ETM+ images. BSMA leads to an improved estimate of subpixel vegetation fractions, and provides uncertainty information for the estimates. The study also found that the traditional SMA using the statistical means of the signature distributions as endmember signatures produces subpixel endmember fractions with almost the same and sometimes even better accuracy than those from BSMA except without uncertainty information for the estimates. However, using the modes of signature distributions as endmembers may result in serious bias in subpixel endmember fractions derived from traditional SMA.
© 2005 Elsevier Inc. All rights reserved.

Keywords: Spectral mixture analysis; Urban remote sensing; Bayes Theorem; Ikonos; Landsat; NDVI

1. Introduction

In the urban environment both quality of life and surface biophysical processes are closely related to the presence of vegetation. Satellite remote sensing provides a retrospective and synoptic view of large areas, thus offering the opportunity to monitor the spatio-temporal dynamics of urban land-use/land-cover (LULC) in a timely and cost-effective manner (Yang & Lo, 2002). Traditional LULC classification, which assigns each pixel to one and only one LULC type, assumes that the spatial extent of LULC components must be larger than the pixel size. In this case, an LULC type is expressed by a group of pixels. Due to the complexity of urban landscape structure, the assumption that each pixel is composed of one and only one LULC type is often not valid for most remotely sensed data. Spectral mixture analysis (SMA) has been frequently used to derive subpixel vegetation information from remotely sensed imagery in urban areas. The essential assumptions for SMA include: (1) the landscape is composed of a few fundamental components, referred to as endmembers, each of which is spectrally distinctive from the others; (2) the spectral signature for each component is a constant within the entire spatial extent of analysis, and (3) the remotely sensed signal of a pixel is linearly related to the fractions of endmember present.

* Tel.: +1 919 843 4764; fax: +1 919 962 1537.
E-mail address: csong@email.unc.edu.

0034-4257/$ - see front matter © 2005 Elsevier Inc. All rights reserved.
doi:10.1016/j.rse.2005.01.002

The key to successful SMA is appropriate endmember selection (Elmore et al., 2000; Tompkins et al., 1997). Selecting endmembers involves identifying the number of endmembers and their corresponding spectral signatures. Though multispectral sensors usually collect remote sensing data at several wavelengths, and hyperspectral sensors take measurements in hundreds of spectral bands, we can only use a very limited number of endmembers in SMA as multispectral remotely sensed data are usually highly correlated. It is the dimensionality of the data, not the number of bands that determines how many endmembers can be used in SMA (Mustard, 1993; Radeloff et al., 1999). In a sensitivity analysis of endmember selection for SMA for subpixel forest cover using Along Track Scanning Radiometer 2 (ATSR-2) imagery collected in summer 1997 in central Finland, Theseira et al. (2003) found that the first principal component of the four-band ATSR-2 imagery accounts for 96.92 percent of the variance of the image data. Therefore, a two-endmember model may be under determined as the solution of subpixel endmember fractions is not unique. Though Landsat Thematic Mapper/ Enhanced Thematic Mapper Plus (TM/ETM+) sensors have six spectral bands, Radeloff et al. (1999) found that a three-endmember (shade, nonphotosynthetic vegetation, and green vegetation) SMA always achieved better results in detecting budworm defoliation than those with four endmembers. Ridd (1995) used a three-endmember vegetation-impervious-soil (VIS) model in Salt Lake City, Utah to characterize urban structure at the subpixel level with Landsat TM data. The same three-endmember model was later applied to Bangkok, Thailand (Madhavan et al., 2001) and Brisbane, Australia (Phinn et al., 2002). Small (2001) identified another three-endmember model, vegetation-low albedo-high albedo (VLH), for spectral mixture analysis in the urban environment after analyzing a time series of Landsat TM images of New York City, New York. More recently, Wu and Murray (2003) modified the VIS model for Columbus, Ohio to be a four-endmember model to accommodate the spectral variability of impervious endmember: vegetation, low albedo, high albedo and soil (VLHS). Smith et al. (1990) found that SMA with three endmembers, vegetation, soils, and shade, can facilitate mapping and monitoring of vegetation cover over large regions in a desert environment with Landsat TM image.

Even with hyperspectral remotely sensed data from an Airborne Visible InfraRed Imaging Spectrometer (AVIRIS), which has 224 spectral bands, the number of endmembers allowed for SMA is often limited. Wessman et al. (1997) used seven endmembers for SMA with AVIRIS data, including nonphotosynthetic vegetation (NPV), shade, soil, rock, and three green vegetation endmembers (representing canopy vertical structure, greenness, and fractional cover of grass, respectively). Okin et al. (2001) only used four endmembers for SMA with AVIRIS data to retrieve vegetation and soil information in an arid and semiarid environment. In a separate study with AVIRIS data, Roberts et al. (1993) found that 98 percent of the spectral variation could be explained by a linear mixture of three endmembers: green vegetation, shade and soil. Statistically, more endmembers lead to better fit of the data when mixing endmembers in the forward direction to produce the composite spectral signal of a pixel, while the opposite is true when unmixing the composite spectral signal in the backward direction to derive subpixel endmember fractions. A minimum number of endmembers that describe the spectral variability of the scene would be the ideal choice for SMA (Sabol et al., 1992).

Once endmembers are defined, the next critical step in SMA is to identify the spectral signatures for the endmembers. This is sometimes the most difficult step (Tompkins et al., 1997). Theseira et al. (2003) summarized various approaches for endmember selection used in the literature. Though the specific techniques for selecting endmembers may differ, the spectral signatures of endmembers are in general derived from two sources: (1) reference endmembers, whose spectral signatures are measured on the ground or in the laboratory with spectroradiometer (Adams et al., 1995; Roberts et al., 1998; Smith et al., 1990), or (2) image endmembers, whose spectral signatures are obtained from the remotely sensed images to be unmixed (Atkinson et al., 1997; Elmore et al., 2000; Ridd, 1995; Wessman et al., 1997). Though reference endmember spectra can be well controlled and accurately measured, they may not match those in the image because of noise caused by numerous factors including sensor differences, atmospheric effects, illumination conditions, and phenology (Song & Woodcock, 2003a). A complicated calibration process is usually required to match the reference spectra with the image spectra (Roberts et al., 2002). Gong and Zhang (1999) advised caution in using reference endmembers because a small percentage of noise in reference endmember spectra can lead to disproportionally large errors in endmember fractions. Image endmembers are often obtained from the pure endmember pixels in the image to be unmixed (Roberts et al., 2002; Souza et al., 2003; Theseira et al., 2003) or from a feature space (Ridd, 1995; Theseira et al., 2003; Wu & Murray, 2003). Obtaining image endmember signatures can sometimes be difficult, as the spectral signature of an endmember may vary significantly (Atkinson et al., 1997; Theseira et al., 2003). Bateson and Curtiss (1996) developed an approach for manual endmember selection from images. However, due to spectral variability different users may generate different sets of endmembers given the same image. Variation in endmember spectral signatures is a fundamental issue in SMA as it leads to poor accuracy in endmember fractions (Carpenter et al., 1999; Petrou & Foschi, 1999; Theseira et al., 2003).

Using a few endmembers to represent the entire landscape is a significant simplification of the real world. It is an even greater simplification to represent each of them with a constant spectral signature. Attempts have been made to explore ways to incorporate the variation of endmember

signatures in SMA. In an effort to extract subpixel land cover types from NOAA-AVHRR NDVI images, Kerdiles and Grondona (1995) took four image windows and derived image endmembers from each window. They found, when the image endmembers from one window were applied for SMA in another window, the accuracy of endmember fractions decreased. They improved the accuracy of endmember fractions using the averaged endmember signatures from all four windows. Roberts et al. (1998) developed a Multiple Endmember Spectral Mixture Analysis (MESMA) to map the subpixel proportion of Chaparral in the Santa Monica Mountains, California where endmembers were dynamically selected from a spectral library containing hundreds of reference endmembers. When the spectral signatures were allowed to vary from pixel to pixel, they found most of the images could be simulated with a two-endmember model.

Hung and Ridd (2002) designed a set of expert system rules and fuzzy maximum likelihood classification for six land cover types on the basis of VIS model in order to account for the intraclass signature variations. They concluded that their mixed accuracy assessment results are primarily caused by the discrete recognition of the continuous phenomena of LULC types. Ju et al. (2003) developed a mixture discriminant analysis algorithm to infer land cover fractions where each class was modeled as a mixture of Gaussian distributed subclasses. They found that using mixture discriminant analysis, which accounts for intraclass variations, outperformed traditional SMA in extracting subpixel fractions of vegetation types. Acknowledging the difficulty in selecting endmembers, Tompkins et al. (1997) developed a modified SMA approach where they treated both the endmember fractions and endmember signatures as unknowns to be solved. Such a treatment makes the equations nonlinear, which could severely limit its operational use due to the complexity involved in solving the nonlinear equations. Bateson et al. (2000) introduced the concept of endmember bundles to incorporate the endmember variability in SMA. Rather than using a single vector, an endmember is represented by a bundle of vectors in spectral space. Bundle unmixing finds the minimum and maximum fractions for each endmember bundle. The average of minimum and maximum endmember fractions is used as the mean fraction for each endmember. The underlying assumption for estimating the mean endmember fractions is that the endmember bundle vectors are uniformly or symmetrically distributed within each endmember bundle domain, which may not be true. More recently, Asner and Heidebrecht (2002) developed a Monte Carlo approach to estimate the uncertainty of subpixel endmember fractions by randomly drawing endmembers from the endmember bundles for SMA, where similar underlying assumption is needed.

It is an essential dilemma in SMA that the continuous variation of endmember signatures demands more endmembers to represent them, while the limited dimensionality of remotely sensed data necessitates fewer endmembers. This paper develops a new SMA technique based on the Bayesian Theorem, along with the traditional SMA techniques, to improve understanding of the impact of endmember variability on the derivation of subpixel vegetation fractions in an urban environment. In Bayesian Spectral Mixture Analysis (BSMA), endmember signatures are no longer treated as constants, but they are represented by probability density/mass functions. The BSMA model developed in this paper can incorporate endmember spectral variability in the unmixing process, thus demanding fewer endmembers, which should improve the accuracy of endmember fractions (Sabol et al., 1992). In this paper, I first develop a two-endmember BSMA (vegetation and nonvegetation) to characterize the urban structure. The theory is then expanded for a three-endmember (vegetation-low albedo-high albedo) BSMA model. Though BSMA is applied to an urban area in this study, its application is not limited to the urban environment.

2. Theoretical background

2.1. Two-endmember BSMA

SMA using two endmembers with constant signatures is the simplest case. Though simple, it is a very useful tool for applications where the objective is to map binary land-cover types, such as vegetation and nonvegetation (Qi et al., 2000) and forest and non-forest (Theseira et al., 2003). However, the two-endmember BSMA model is much more flexible than the traditional two-endmember SMA. It works similarly to MESMA (Roberts et al., 1998), as each pixel is unmixed with all possible different combinations of endmember signatures. The difference is that BSMA takes into account the probabilities of spectral signatures, while MESMA assumes equal probabilities for all endmembers.

Fig. 1 illustrates the variability of endmember spectral signatures of vegetation and nonvegetation derived from an Ikonos image for Bangkok, Thailand. The dashed lines define the one-dimensional space of Normalized Difference Vegetation Index (NDVI) in the two-dimensional Red/Near-Infrared space. At 4×4 m spatial resolution, NDVI can separate vegetation and nonvegetation well, but each spans a wide range of NDVI in which the endmembers are not uniformly distributed. In the two-dimensional Red/Near-Infrared space, vegetation and nonvegetation each span an elongated ellipse. The triangle envelope, which is formed by the vegetation and nonvegetation, is the physical basis for SMA using VLH endmembers (Small, 2003). Nonvegetation features distribute in the Red/Near-infrared space primarily along the soil line. The signature variation for nonvegetation is primarily due to differences in physical composition (such as bare soil, concrete roads or parking lots, and rooftops) and moisture conditions. Urban vegetation types, whose biophysical and biochemical composition

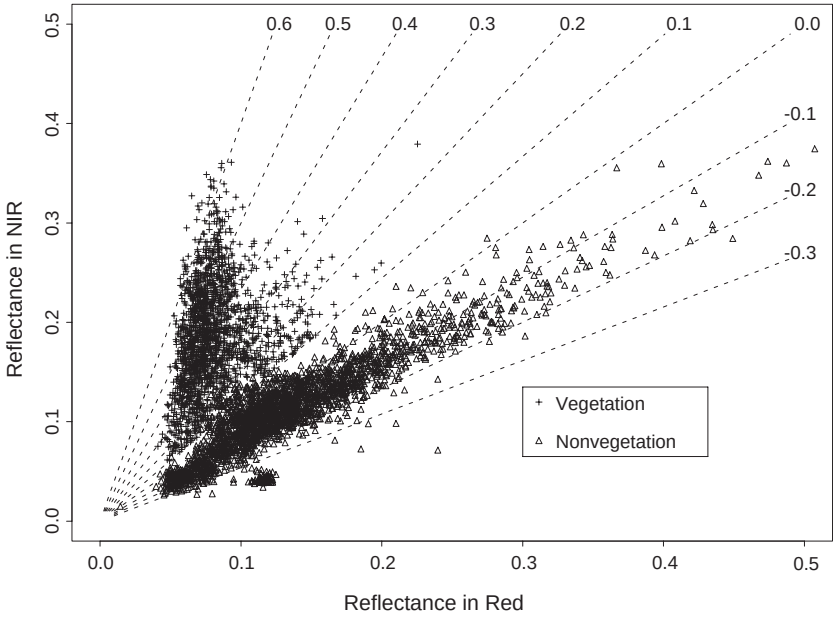

Fig. 1. Spectral variation for vegetation and nonvegetation derived from an Ikonos image collected on Nov 27, 2002 over Bangkok, Thailand. The dashed lines are NDVI isolines with values marked at the end of the line. In one-dimensional space, NDVI provides very good separation for the two endmembers. But each endmember spans a wide range of NDVI values, in which they are not uniformly distributed. In the Red/Near-infrared space, we see the scatter points form a triangular envelope, which is the physical basis for vegetation-low albedo-high albedo (VLH) model. The challenge for traditional SMA is to identify endmember signatures that can be treated as constants for spectral mixture analysis while the endmember signatures vary continuously in spectral space.

can vary greatly, often produce very different spectral signatures (Asner, 1998). Moreover, components of urban vegetation endmember are not uniformly distributed in the spectral space. At a coarser spatial resolution, any point in the vegetation region can combine with another point in the nonvegetation region to produce a mixture signal. Such a situation poses a significant challenge for endmember selection in traditional SMA. However, endmember variability is incorporated in BSMA, as the signature of each endmember is represented by a probability function over its entire feature space. In BSMA, each point in the vegetation signature space is allowed to mix with any point in the nonvegetation signature space in Fig. 1.

Due to the unity constraint for endmember fractions, we only need a single spectral measurement for traditional SMA with two endmembers as long as they have distinct spectral signatures. In this study, NDVI is used for spectral mixture analysis with two endmembers because of its sensitivity to the presence of vegetation (Fig. 1) and its common use in extracting land surface biophysical parameters. In fact, BSMA can be used with any other spectral measurements. Despite concerns of nonlinear interactions of photons among the endmembers (Elvidge & Lyon, 1985; Huete et al., 1985; Ray & Murray, 1996), NDVI is frequently used in SMA (Defries et al., 2000; Hanan et al., 1991; Kerdiles & Grondona, 1995; Qi et al., 2000). In general, linear mixing predominates the nonlinear interactions for NDVI values of mixed pixels (Garcia-Haro et al., 1996). A recent study found that NDVI is nonlinearly related to vegetation fraction when dense healthy vegetation is mixed with dark backgrounds (Song, 2004). Therefore, it is not appropriate to use NDVI in SMA to derive subpixel green canopy fractions for forest stands as the scenes would be primarily composed of bright green canopy and dark shadows only. NDVI is linearly related to subpixel vegetation fractions when the background is brighter. Thus it is reasonable to use NDVI to extract subpixel vegetation fractions in urban environments.

Traditional two-endmember SMA with NDVI can be written as

$$c^{*}\mathrm{NDVI}_{\mathrm{v}} + (1.0 - c)^{*}\mathrm{NDVI}_{\mathrm{u}} = \mathrm{NDVI}_{\mathrm{m}} \quad (1)$$

where $\mathrm{NDVI}_{\mathrm{v}}$ and $\mathrm{NDVI}_{\mathrm{u}}$ are NDVI values for pure vegetation and nonvegetation pixels, respectively. $\mathrm{NDVI}_{\mathrm{m}}$ is the NDVI value for the mixed pixel. The parameter of interest, c, is subpixel vegetation fraction ranging from 0.0 to 1.0. For example, given $\mathrm{NDVI}_{\mathrm{v}}$=0.8 and $\mathrm{NDVI}_{\mathrm{u}}$=−0.2, the vegetation fraction c is equal to 0.7 with $\mathrm{NDVI}_{\mathrm{m}}$=0.5. However, the situation in the real world is not as simple. The spectral signatures of both vegetation and nonvegetation can change significantly within any sizable urban area. Suppose we have a 20 percent decrease in the brightness of the vegetation signature in the example above; the 20 percent decrease in the vegetation signature would propagate to the vegetation fraction as errors, leading to c=0.83, if we continue to assume the same spectral signature for vegetation. In reality, if we pool together all the "pure" pixels of an endmember in an image, what we have is a population of signatures for the endmember, as we see in Fig. 1.

Assuming the NDVI probability density functions are $f_{\mathrm{v}}(\mathrm{NDVI})$ and $f_{\mathrm{u}}(\mathrm{NDVI})$ for vegetation and nonvegetation,

respectively, the solution for Eq. (1) is not unique. For any given c, there are many choices of combinations for $NDVI_v$ and $NDVI_u$ that lead to $NDVI_m$. Moreover, the likelihoods of the choices are different. In fact,

$$f(\mathrm{NDVI_m}|c) = f_v(\mathrm{NDVI}) \otimes f_u(\mathrm{NDVI_m} - c^*\mathrm{NDVI}) \quad (2)$$

where $f(\mathrm{NDVI_m}|c)$ is the conditional probability density function of NDVI for a mixed pixel at a given vegetation fraction. The symbol "⊗" denotes convolution of f_v with f_u. However, what we are really interested in for SMA is the probability of subpixel vegetation fractions at a given $NDVI_m$, i.e. $p(c|\mathrm{NDVI_m})$. Based on Bayes Theorem (Drake, 1967; Salvucci & Song, 2000),

$$p(c|\mathrm{NDVI_m}) = \frac{f(\mathrm{NDVI_m}|c) \times \pi(c)}{\int_0^1 f(\mathrm{NDVI_m}|u)\pi(u)du} \quad (3)$$

where $f(\mathrm{NDVI_m}|c)$ is given in Eq. (2), and $\pi(c)$ is the prior probability density function of subpixel vegetation fractions for any pixel in the image. The prior probability, $\pi(c)$, should be a uniform distribution with c ranging from 0.0 to 1.0 before we know anything about a pixel. In contrast to the deterministic endmember fractions from traditional SMA, BSMA leads to a probability mass function of subpixel vegetation fractions for each pixel. Therefore, we cannot only derive the expected subpixel vegetation fractions, but also the uncertainty information associated with the estimates.

When there are multiple spectral measurements available, BSMA, as shown in Eq. (3), can be recursively used to further refine our estimates as in the following:

$$f'(c|\mathrm{DN_m}) = \frac{f(\mathrm{DN_m}|c) \times p(c)}{\int_0^1 f(\mathrm{DN_m}|u)p(u)du} \quad (4)$$

where $p(c)$ is the probability of subpixel endmember fractions obtained from the first spectral measurement. This process can continue with each recursion adding the new information from an additional spectral measurement to refine the estimate of subpixel endmember fractions. However, multispectral remotely sensed data often contain significant redundant information. It is computationally expensive and unnecessary to recursively use Eq. (4) for each band. Information from remotely sensed data should be compressed into fewer dimensions with some orthogonal transformation before using Eq. (4).

2.2. Three-endmember BSMA

A significant advantage of BSMA developed in this paper is the ability to incorporate the intraclass variability of the spectral signatures in the unmixing process. Intraclass variability of remotely sensed data is often too high to allow a unique unmixing of a single pixel (Petrou & Foschi, 1999). In Fig. 1, we can see three endmembers (vegetation, low albedo and high albedo features) in the Red/Near-infrared space. The low albedo feature is relatively concentrated in the spectral space, while the vegetation and high albedo features vary significantly. Selecting the endmembers whose signatures will be used as constants remains a challenge in traditional SMA. Here the two-endmember BSMA is expanded to incorporate three endmembers.

For SMA with three endmembers, we need at least two independent spectral measurements: R_1 and R_2. The linear mixture equations can be written as

$$\begin{cases} c_1R_{11} + c_2R_{12} + (1.0 - c_1 - c_2)R_{13} = R_1 \\ c_2R_{21} + c_2R_{22} + (1.0 - c_1 - c_2)R_{23} = R_2 \end{cases} \quad (5)$$

where R_{ij} denote the spectral signature of endmember j for spectral measurement i. The objective of SMA is to obtain c_1 and c_2 from Eq. (5). The solution is straightforward when the endmember signatures, R_{ij}, are constants. Due to endmember variability, there are many different combinations of endmembers that lead to the same spectral measurements for any given set of R_1 and R_2 though the likelihood of having each combination varies. The solution becomes probabilistic, i.e. when the endmember signatures follow probability distributions within certain domains. $p(c_i|R_1R_2)$, where the subscript i=1 or 2. Based on Bayes Theorem (Carlin & Louis, 1996), we have

$$p(c_i|R_1R_2) = \frac{f(R_2|c_i)g(c_i|R_1)}{\int_0^1 f(R_2|u)g(u|R_1)du} \quad (6)$$

where

$$g(c_i|R_1) = \frac{f(R_1|c_i)h(c_i)}{\int_0^1 f(R_1|u)h(u)du} \quad (7)$$

where $f(R_1|c_i)$ and $f(R_2|c_i)$ can be obtained from Eq. (5) through convolutions similar to Eq. (3). Again, Eq. (6) can be recursively used as in Eq. (4) if there are more than two independent spectral measurements available.

3. Methods

3.1. BSMA with simulated images

Simulated images provide a useful source of data for improving our understanding of information extraction from remotely sensed data, and thus they are frequently used in remote sensing studies (Asner et al., 1997; Song & Woodcock, 2003b; Townshend et al., 1992). The advantage of using simulated mixture image in this study is that the exact endmember fractions are known. An additional advantage of using simulated images here is that the non-linear interactions of photons among endmembers do not exist, simplifying the problem and allowing better under-

standing of the impact of endmember variability on SMA. In this study, BSMA is applied to three sets of simulated mixture images, each of which has a dimension of 100×100 pixels. The first set contains a single simulated mixture image which is generated based on a two-endmember model: vegetation/nonvegetation. The endmember spectral signatures are assumed to follow Gaussian distributions with a mean NDVI of 0.3 and a standard deviation of 0.12 for vegetation, and a mean NDVI of −0.1 and a standard deviation of 0.08 for nonvegetation (Fig. 2), respectively. The mixture image is generated in two steps. First, a subpixel vegetation fraction image is generated using a Monte Carlo simulation, assuming a Gaussian distribution with a mean of 0.5 and a standard deviation of 0.15 for the subpixel vegetation fractions for the 100×100 pixels. Second, the mixture NDVI image is produced according to Eq. (1) for each of the 100×100 pixels where the subpixel vegetation fractions are generated in the first step, and the vegetation endmember and the nonvegetation endmember are randomly drawn from their respective probability distributions. Thus, the subpixel vegetation fractions are known for each pixel of the mixture image. The mixture image is then unmixed with BSMA using the entire probability distribution of the endmembers. As a comparison, the mixture image is also unmixed with traditional SMA, in which the means of the endmember signature distributions are used as endmember signatures.

The second set also consists of a single mixture image which is generated in the same way as the first one, except the endmember signatures no long follow Gaussian distributions. Instead, the endmembers follow skewed probability density functions as shown in Fig. 3. The probability density for the nonvegetation endmember linearly increases from 0 at NDVI=−0.3 to its peak at NDVI=−0.22, and linearly decreases to 0 at NDVI=−0.1. The probability density for the vegetation endmember linearly increases from 0 at NDVI=0.1 to its peak at NDVI=0.5, and linearly decreases to 0 at NDVI=0.7. In both Figs. 2 and 3, the areas underneath the probability density curves integrate to unity. The mixture image is unmixed with BSMA using the probability density functions for endmember signatures. For comparative purposes, the mixture image is also unmixed with traditional SMA, in which the means and modes of the signature distributions are used as the endmembers.

The third set includes two mixture images generated for BSMA with three endmembers as shown in Eq. (6). SMA with three endmembers requires a minimum of two independent spectral measurements. The mixture images, which are assumed to be raw DNs from the red and near-infrared spectra, are generated based on the VLH urban structure model. This model assumes that the urban landscape consists of vegetation, low albedo and high albedo features. The probability mass function of endmember spectral signatures in the two bands are shown in Fig. 4, where vegetation has low reflectance in red and high reflectance in near-infrared, while the low albedo features have low reflectance in both bands, and high albedo features have high reflectance in both spectra. The mixture images are generated in two steps. First, endmember fraction images are generated assuming the interpixel variations of endmember fractions follow Gaussian distributions with means of 0.4 and 0.3 and standard deviations of 0.15 and 0.1 for vegetation and low albedo endmembers respectively, and the remaining fractions as the high albedo endmember.

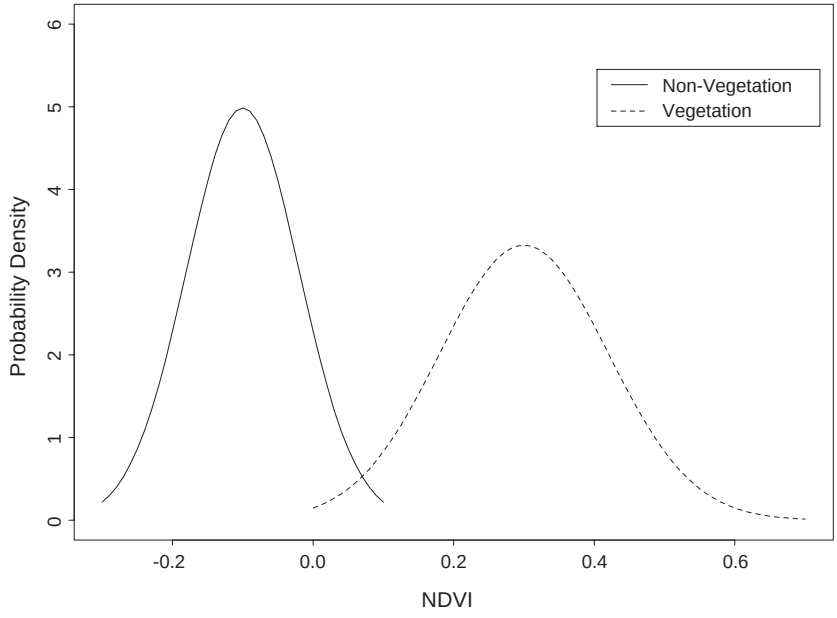

Fig. 2. Hypothetical signature probability density functions for vegetation and nonvegetation. NDVI values for both endmembers are normally distributed with means of 0.3 and −0.1 and standard deviations of 0.12 and 0.08 for vegetation and nonvegetation, respectively. The area underneath each curve integrates to unity.

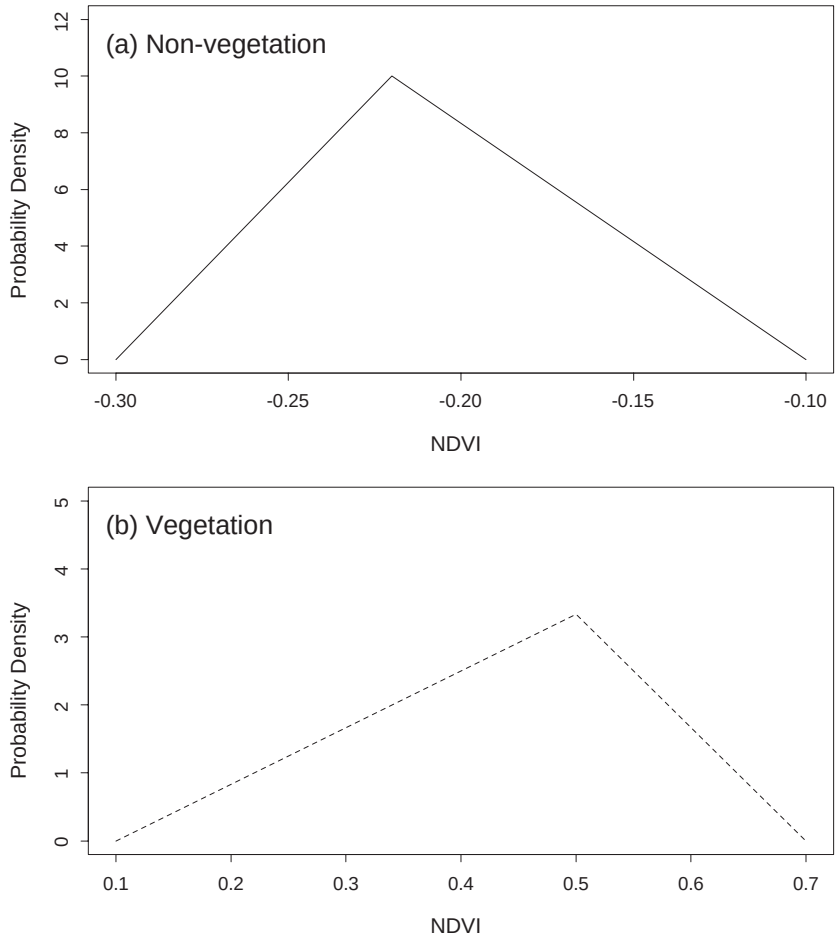

Fig. 3. Hypothetical NDVI probability density functions for vegetation and nonvegetation. The probability for nonvegetation endmember linearly increases from 0 at NDVI=−0.3 to its peak at NDVI=−0.22, and linearly decreases to 0 at NDVI=−0.1. The probability for a vegetation endmember linearly increases from 0 at NDVI=0.1 to its peak at NDVI=0.5, and linearly decrease to 0 at NDVI=0.7. The probability density function for all NDVIs integrates to unity for each endmember.

Second, mixture images are generated according to Eq. (5) where the signature for each endmember is drawn from the probability mass functions shown in Fig. 4. The mixture images are unmixed with BSMA using Eq. (6). In addition, traditional SMAs are also performed using the means and modes of the endmember signature distributions.

3.2. BSMA with real images

Two spaceborne remotely sensed images covering Bangkok, Thailand are used in this study. The first is an Ikonos image, which was collected on November 27, 2002. The viewing elevation and azimuth angles for the Ikonos image were 74.2° and 66.1°, respectively. The second is a Landsat ETM+ image, which was collected on November 16, 1999. Due to the difficulty in accurately obtaining the endmember signatures, BSMA with real images is performed with two endmembers only: vegetation/nonvegetation. BSMA is first applied to the Ikonos image and then applied to the Landsat image. In both cases, the spectral signatures of vegetation and nonvegetation are derived from the Ikonos image at 4×4 m spatial resolution (Fig. 1). The spectral measurements of Ikonos are converted to at-satellite reflectance. First, the 11-bit image is converted to at-satellite radiance (mw/cm^2/sr=DN) based on the following:

$$L_i = \frac{\mathrm{DN}_i}{K_i} \tag{8}$$

where K_i is a constant for converting 11-bit Ikonos data to at-satellite radiance for band i (http://www.spaceimaging.com/products/ikonos/spectral.htm). Second, the at-satellite radiance is converted to at-satellite reflectance according to:

$$\rho_i = \frac{\pi L_i d^2}{E_i \cos(\theta)} \tag{9}$$

where the subscript i denotes band; d is the Earth–Sun distance in astronomical units, which can be omitted when calculating NDVI as it is canceled; θ is solar zenith angle at the time of image acquisition. E_i is solar constant which is calculated based on the Planck's law and the spectral response function for each band assuming a solar temper-

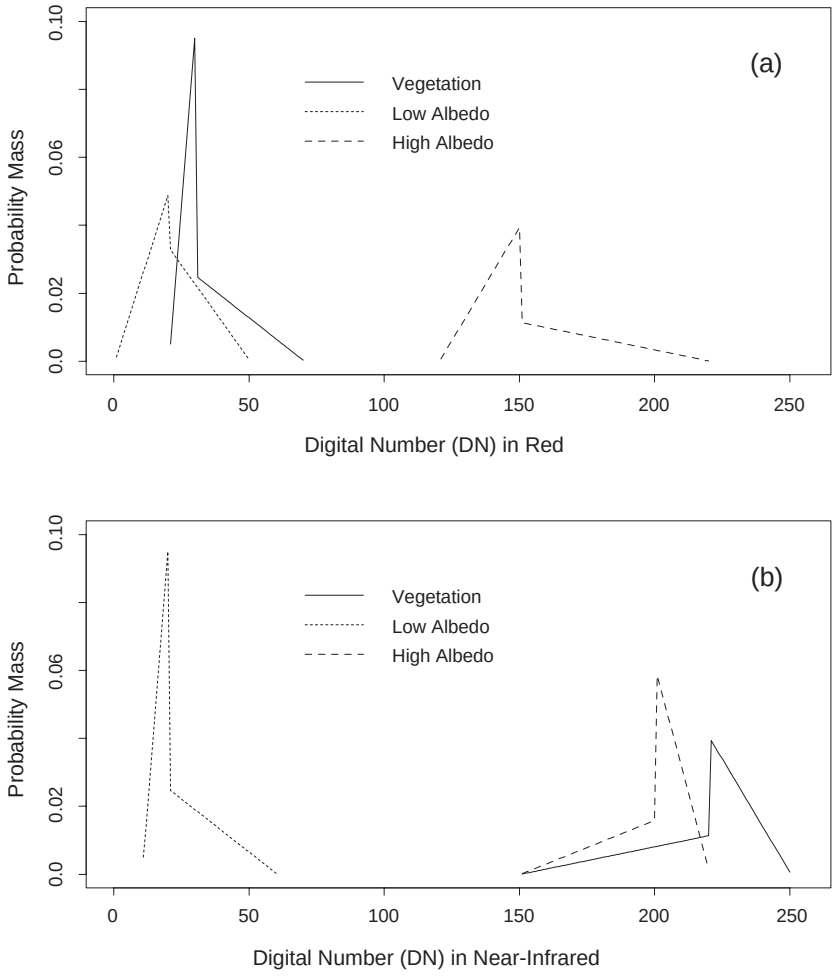

Fig. 4. Spectral signature distributions for three endmembers. (a) Probability mass functions for the signatures of the three endmembers in the red spectrum; (b) probability mass functions for the signatures of the three endmembers in the near-infrared spectrum. The probability mass over the entire range of DNs sum to unity for each endmember in each band.

ature of 5900 K. After the DN values are converted to at-satellite reflectance, NDVI is calculated as

$$\mathrm{NDVI} = \frac{\rho_{\mathrm{nir}} - \rho_{\mathrm{red}}}{\rho_{\mathrm{nir}} + \rho_{\mathrm{red}}} \tag{10}$$

where ρ_{red} and ρ_{nir} are reflectance for the red and near-infrared bands, respectively.

Recent studies found that the characteristic scale of urban reflectance is between 10 to 20 m (Small, 2003). Therefore, most 4×4 m Ikonos multispectral pixels can be assumed spectrally homogeneous. In this study, the 4×4 m Ikonos pixel is classified as either vegetation or nonvegetation, and they are used as endmembers. The multispectral Ikonos image is first classified into 50 spectral clusters through unsupervised classification, and then each cluster is reclassified as vegetation or nonvegetation based on visual inspection assisted with the Ikonos 1-m panchromatic image. With the vegetation/nonvegetation endmember image, we can derive the spectral signatures of NDVI for each endmember. For the convenience of comparison with further analysis using the Landsat ETM+ image, the 4×4 m Ikonos image is degraded to 30×30 m spatial resolution. The endmember map at 4×4 m spatial resolution is also degraded to 30×30 spatial resolution to produce reference subpixel endmember fractions. The degraded NDVI image at 30×30 m spatial resolution is unmixed for subpixel endmember fractions with BSMA using the entire endmember probability distribution of NDVI as well as the traditional SMA with constant endmembers that take the values of the means and modes of the endmember signature distributions, respectively.

Though vegetation and nonvegetation can be fairly easily separated in Ikonos imagery, one Ikonos scene only covers 11×11 km. In addition, Ikonos imagery only became available recently. Landsat images provide a much longer historical archive and larger spatial extent, thus they are among the most frequently used images for SMA over urban areas (Ward et al., 2000). In this study, BSMA is applied to the Landsat 7 ETM+ data for the same area where the Ikonos image was collected. Though the Ikonos image was collected 3 years later, they both were taken in the same month. A recent study showed that the

endmember spectral signatures from an Ikonos image, after cross-sensor calibration, can be used for SMA of the Landsat ETM+ image (Song, 2004). The essence of the calibration includes two steps. First, the satellite measurements in different radiometric resolutions are converted into absolute physical measurements, i.e. at-satellite reflectance. Conversion of the Landsat ETM+ raw image to at-satellite reflectance is similar to that applied to the Ikonos image, as shown in Eq. (9). Second, the histograms of the spectral measurements are matched at the same spatial resolution, i.e. degrading the Ikonos image to the spatial resolution of the Landsat ETM+ image. The histogram of the degraded Ikonos NDVI image is then matched with the Landsat ETM+ NDVI image of the same area. The NDVI image from Landsat is unmixed with BSMA using the endmember signature distributions from the Ikonos image generated at 4×4 m spatial resolution. The reference endmember fraction map derived from the Ikonos image is used for validation. Again the traditional SMA, using the means and modes of the endmember signature distributions, are performed for the purpose of comparison.

4. Results

4.1. Simulated two-endmember models

Fig. 5 shows the vegetation endmember fractions unmixed from the simulated vegetation/ nonvegetation mixture image, in which endmember signatures are assumed to follow Gaussian distributions. The vegetation endmember fractions from the traditional SMA using the means of the endmember signature distributions are given in Fig. 5a as a comparison to the vegetation endmember fractions from BSMA in Fig. 5b. The unmixing results from the two algorithms look very similar. However, the traditional SMA tends to have a higher error when the actual vegetation fractions are either low or high, and a small number of pixels even have endmember fractions 0 and 1. This is because the traditional SMA does not account for the variation in endmember signatures while the simulated image allows the endmember signatures to change from pixel to pixel. When the actual endmember signatures are significantly different from the endmember signatures used,

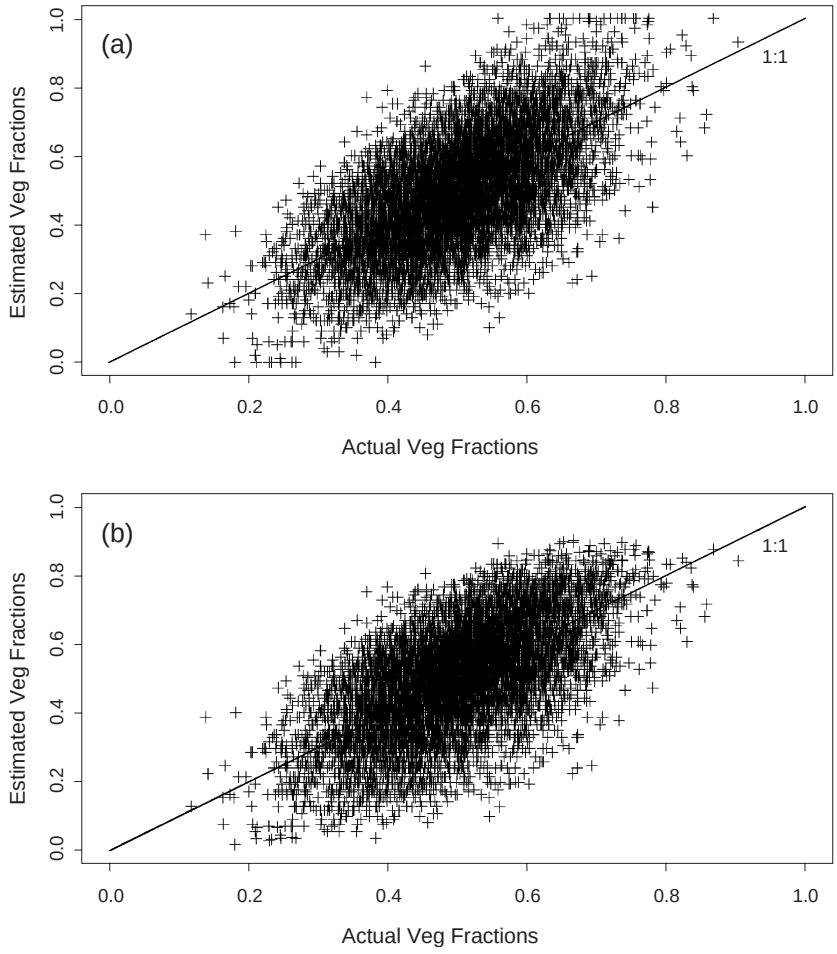

Fig. 5. Results of spectral mixture analysis for subpixel vegetation fractions from the simulated image with vegetation/nonvegetation signature shown in Fig. 2: (a) SMA using the means of endmember signature distributions (RMSE=0.12), and (b) BSMA using the entire signature distribution (RMSE=0.11). Both algorithms lead to an unbiased estimate of subpixel vegetation fractions, but the traditional spectral mixture analysis has a wider range of uncertainty.

the errors propagate to the endmember fractions. The errors are more visible in Fig. 5 when the actual vegetation fractions are either low or high than when they are at intermediate level. Endmember fractions are forced to be 0 or 1 if they are less than 0 or greater than 1 from the unmixture analysis. Such a phenomenon does not occur with BSMA as it allows the endmember signatures to vary conditioned on the NDVI given. The variability of endmember signatures is accounted for by the endmember signature probability distributions in BSMA, reducing the errors at high or low vegetation fractions. Further analysis found that the subpixel vegetation fractions based on the traditional SMA approach have a slightly larger root-mean-squared error (RMSE=0.12) than those from BSMA (RMSE=0.11).

The subpixel vegetation fractions in Fig. 6 are derived from the mixture images with the endmembers following skewed probability distributions as shown in Fig. 3. BSMA and traditional SMA using the signature means lead to more accurate subpixel vegetation fractions than SMA using the modes in this case. SMA using the modes of the endmember distribution generally leads to an overestimate of subpixel vegetation fractions (Fig. 6a). This implies that SMA using signatures from the most commonly seen vegetation/non-vegetation features may not be the best choice for endmembers. SMA using the means of the endmember distribution (Fig. 6b) and BSMA (Fig. 6c) lead to improved estimates of subpixel vegetation fractions. Similar to the generated images with Gaussian endmember signatures, the unmixed subpixel vegetation fractions from BSMA has a smaller range of uncertainty than those from SMA using the means. An additional advantage of BSMA is that we cannot only retrieve the unbiased estimates of subpixel vegetation fractions, but also the standard deviation associated with each estimate. Fig. 6d shows that the uncertainties of estimated subpixel vegetation fractions are low for either

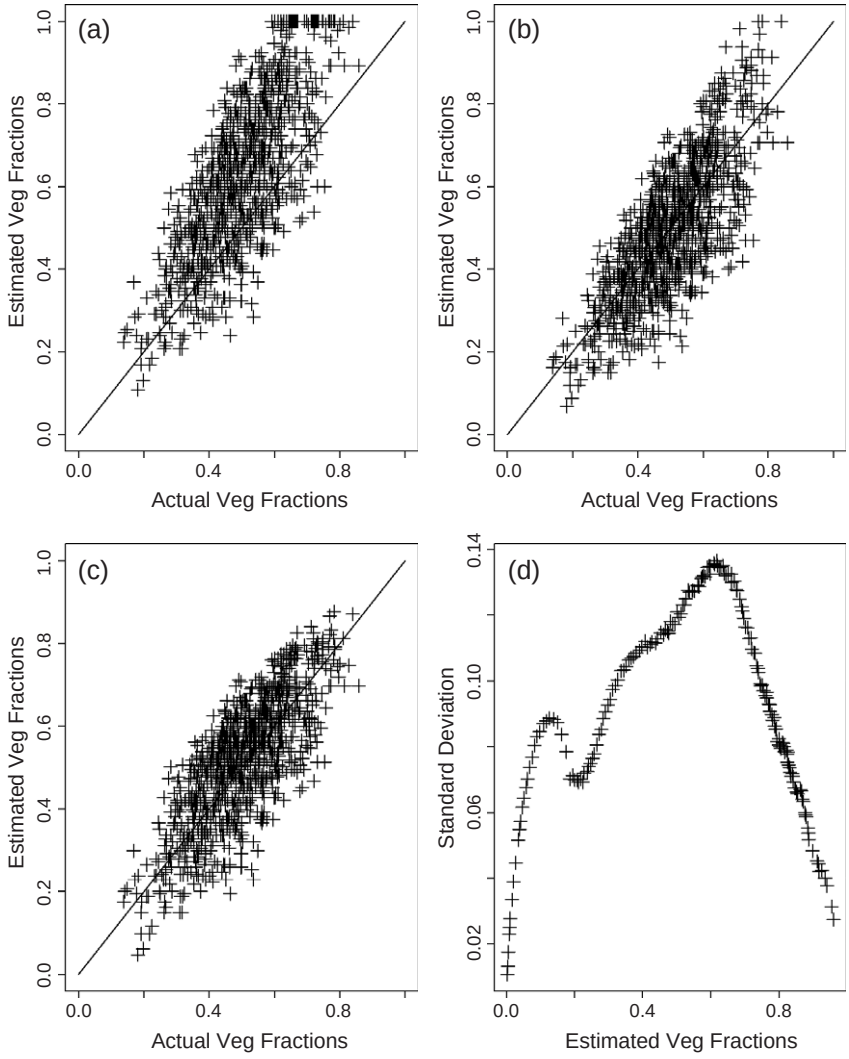

Fig. 6. Spectral mixture analysis for subpixel vegetation fractions from generated images with vegetation/nonvegetation signatures illustrated in Fig. 3: (a) SMA using the modes of the distributions in Fig. 3 (RMSE=0.18); (b) SMA using the means of the distributions in Fig. 3 (RMSE=0.11); (c) BSMA using the entire signature distributions in Fig. 3 for endmember spectral signatures (RMSE=0.10); (d) standard deviations of subpixel vegetation fractions from BSMA.

very high or very low vegetation fractions in the pixel. Uncertainties of subpixel vegetation fractions are high for pixels with an intermediate amount of vegetation, where many different combinations of subpixel vegetation/non-vegetation can produce the same remote sensing signal as a result of endmember variations. Such information is not available from traditional SMA.

4.2. Actual two-endmember models

Vegetation fractions from spectral mixture analysis with the degraded Ikonos multispectral image at 30×30 m spatial resolution are given in Fig. 7. Traditional SMA using modes of the endmember signature distributions as the endmember signatures continues to be the worst case scenario (Fig. 7a). RMSE is 0.11 and 0.13 for subpixel vegetation fractions within the range of [0.0, 1.0] and [0.1, 0.9], respectively. The comparison of SMA using the means of signature distributions as the endmembers with BSMA is not as straight forward. BSMA underestimates the number of pure pixels. Due to the variation of endmember signatures, it produces endmember fractions very close to, but not exactly, pure pixels. This phenomenon did not occur in the analyses of simulated images as the simulation did not generate pure pixels at the conditions given. Therefore, BSMA has a larger RMSE (0.09) over the entire range of vegetation fractions [0.0,1.0] than that (RMSE=0.07) from SMA using the means. Only when RMSE is calculated over the range of [0.1,0.9] for subpixel vegetation fractions, does BSMA have a slightly smaller RMSE (0.07) than that (0.09) from SMA using the means. Therefore, unless the uncertainties of endmember fractions are of interest, SMA using the signature means should be preferred as it is also much simpler than BSMA. Similar to Fig. 6d, errors in subpixel vegetation fractions are smaller for pixels with either very high or very low fractions of vegetation (Fig. 7d).

Results of spectral mixture analysis of Landsat ETM+ NDVI image using endmember signatures from Ikonos image cannot be validated with the subpixel vegetation fractions generated from the Ikonos image on a pixel-by-pixel basis due to geometric registration errors. A small mismatch in the registration can lead to large errors (Dai & Khorram, 1998; Townshend et al., 1992). To reduce the impacts of registration errors on the validation, the vegetation fractions unmixed from the Landsat ETM+ NDVI are compared with the Ikonos vegetation fractions on a window basis. Eight 300×300 windows containing a wide range of vegetation cover are taken from the Ikonos 4×4 m spatial resolution image. In general, the geometric registration accuracy can rarely be better than 0.5 pixels. This implies that the impact of registration error on the validation results could be as high as 75 percent on a pixel-by-pixel basis. With the same registration accuracy, the impact of the geometric error on validation would be 2.5 percent on a window basis with its size given above. Fig. 8 shows the sub-pixel vegetation fractions from the three unmixing scenarios. Subpixel vegetation fractions derived from SMA using the means of the endmember distributions and BSMA using the entire distributions remain more

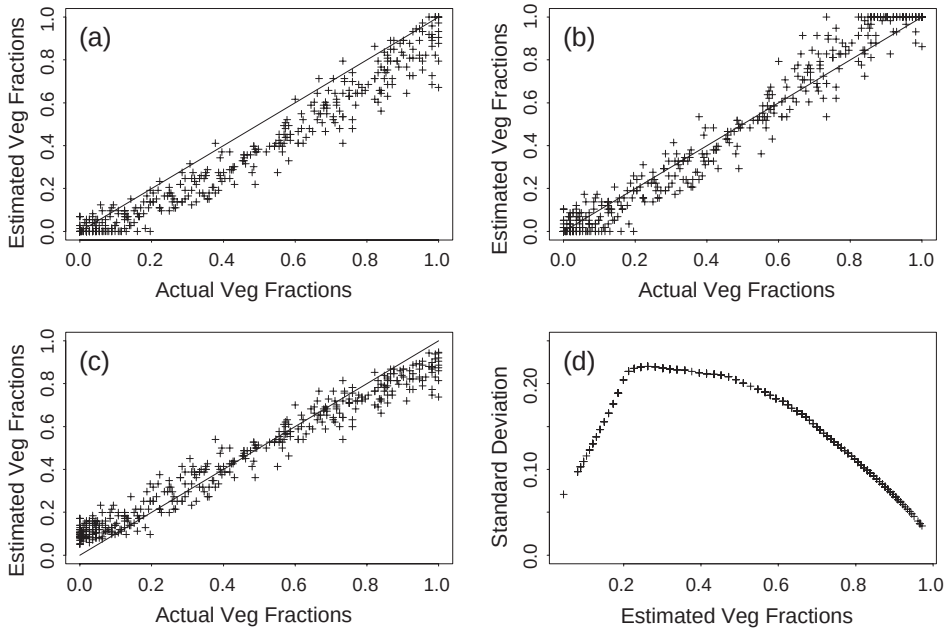

Fig. 7. Spectral mixture analysis for subpixel vegetation fractions using Ikonos NDVI image degraded to 30×30 m spatial resolution: (a) SMA using the modes of endmember signature distributions (RMSE=0.11 for subpixel vegetation fractions from 0.0 to 1.0, and RMSE=0.13 for subpixel vegetation fractions from 0.1 to 0.9); (b) SMA using the means of endmember signature distributions (RMSE=0.07 for subpixel vegetation fractions from 0.0 to 1.0, and RMSE=0.09 for cover from 0.1 to 0.9); (c) BSMA using endmember signature distributions (RMSE=0.09 for subpixel vegetation fractions from 0.0 to 1.0, and RMSE=0.07 for cover from 0.1 to 0.9); (d) standard deviation for subpixel vegetation fractions from BSMA.

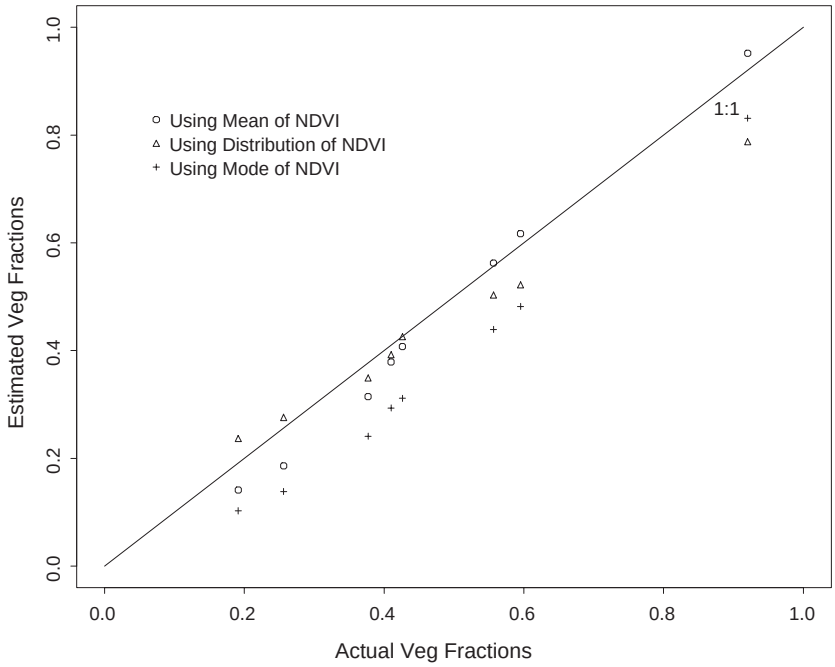

Fig. 8. Validation for the spectral mixture analysis on a window basis. The estimated vegetation fractions are the average vegetation fractions from a 40×40 pixel window at Landsat ETM+ spatial resolution (30×30 m). The actual vegetation fractions are the average vegetation fractions from a window of 300×300 pixels at spatial resolution of Ikonos multi-spectral imagery (4×4 m).

accurate than those from SMA using the modes of the distributions. RMSE is 0.04, 0.06 and 0.11 for subpixel vegetation fractions from the SMA using the means of the distribution, BSMA and SMA using the modes of the endmember distributions, respectively. Again SMA using means of endmember signature distributions produces

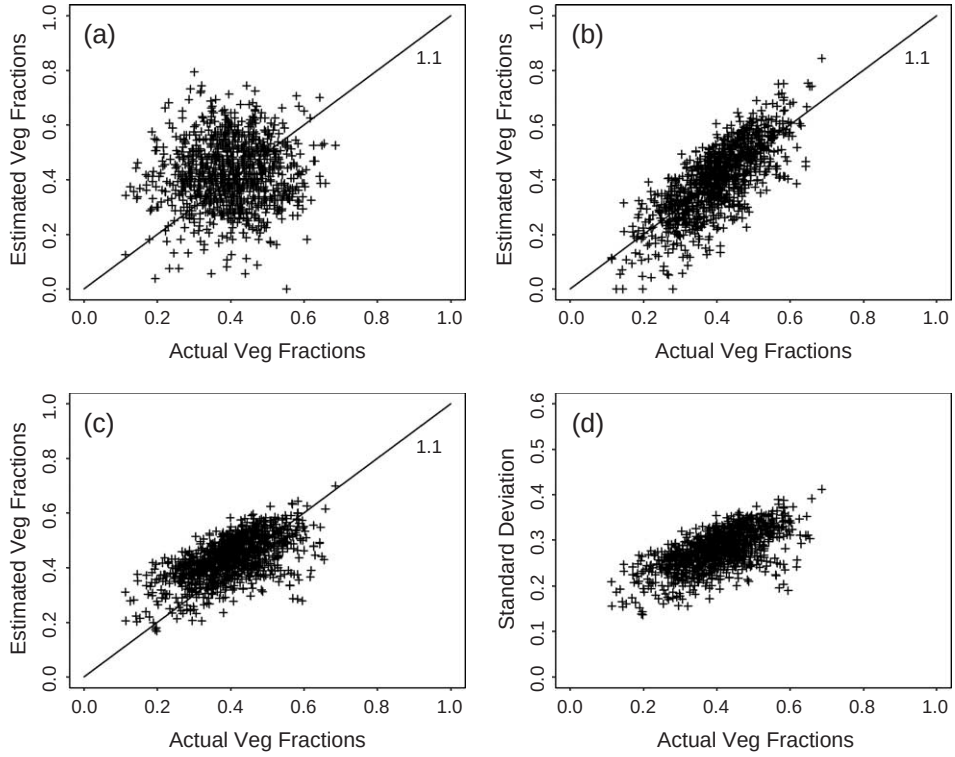

Fig. 9. Spectral mixture analysis results with three endmembers: (a) subpixel vegetation fractions from SMA using modes of the three endmember signature distributions as the endmembers; (b) subpixel vegetation fractions from SMA using means of the endmember signature distributions as the endmembers; (c) subpixel vegetation fractions from BSMA using the entire endmember signature distributions as in Fig. 4; (d) the standard deviation of subpixel vegetation fractions from BSMA.

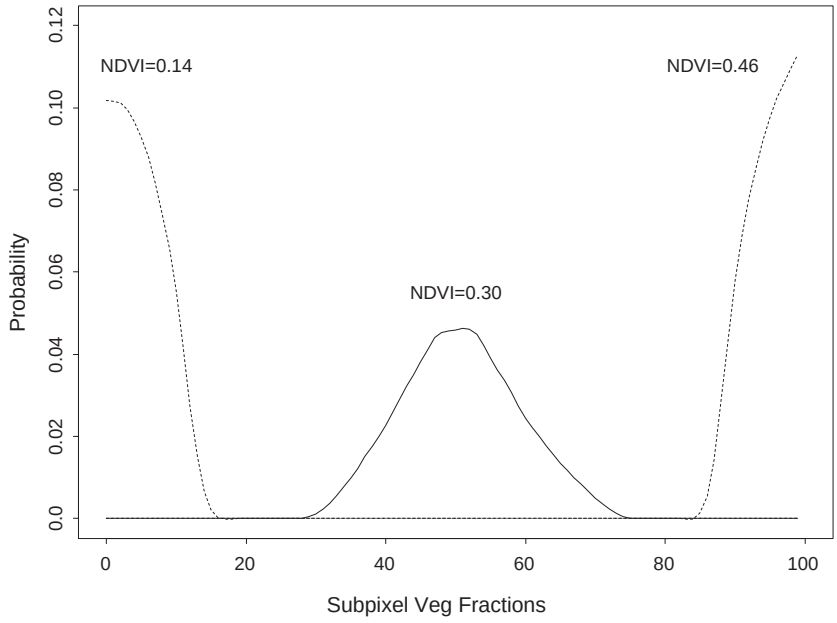

Fig. 10. The probability of subpixel vegetation fractions at given NDVI values. The uncertainty of subpixel vegetation fractions is highest at intermediate vegetation cover as it allows many different combinations of vegetation/nonvegetation fractions to make up the same NDVI value.

smaller RMSE values for endmember fractions compared with those from BSMA. This is primarily caused by the underestimate of pure pixels by BSMA.

4.3. The three-endmember case

The subpixel vegetation fractions unmixed from three-endmember mixture images are shown in Fig. 9. Subpixel vegetation fractions derived using modes of signature distributions remain the least accurate case (RMSE=0.16). BSMA and SMA using the means of the signature distributions as endmembers produce similar results (RMSE=0.09 for both). However, the range of subpixel vegetation fractions from SMA using means of signature distributions is much larger than that from BSMA. We can also see that the standard deviations for vegetation fractions are much larger with three endmembers as compared to Fig. 6d because there are many more possibilities for different endmember combinations that lead to the same remote sensing signal in Eq. (5). We also see that the uncertainty does not decrease at high subpixel vegetation fraction as in the two-endmember case. This is probably due to the overlap of the vegetation spectral signature with the other two endmembers. This further confirms findings in the literature that having more endmembers in SMA is not always advantageous (Radeloff et al., 1999; Sabol et al., 1992).

5. Discussion

This paper developed a new technique, Bayesian Spectral Mixture Analysis (BSMA), to incorporate endmember signature variability in the process of deriving subpixel vegetation fractions in the urban environment. The output of BSMA is no longer deterministic endmember fractions for a pixel, but a probability distribution of subpixel vegetation fractions for each endmember. Thus we have uncertainty information for the estimates, which is not available from traditional SMA. Fig. 10 shows the conditional probabilities of subpixel vegetation fractions derived from the Landsat ETM+ image at three NDVI values, i.e. $f(c|\mathrm{NDVI})$. At NDVI=0.14, the probability decreases as subpixel vegetation fractions increase, and eventually becomes zero, meaning vegetation fractions higher than this are impossible with the low NDVI value. At NDVI=0.46, the probability of lower subpixel vegetation fractions decreases, and finally becomes zero, indicating it is impossible to have lower subpixel vegetation fractions at this high NDVI value. At either very high or very low NDVI values, the probability distributions for subpixel vegetation fractions are very skewed within a narrow range. At an intermediate NDVI value the probability distribution of subpixel vegetation fractions is much more symmetrical and spans a wider range, indicating many different combinations of vegetation and nonvegetation fractions can lead to the same NDVI value. This explains why the uncertainties in subpixel vegetation fractions are low at either very high or very low NDVI values and high at intermediate NDVI values as shown in Figs. 6d and 7d.

Traditional SMA, using the means of endmember signatures, can produce endmember fractions almost as good as, and sometimes even better than those BSMA produces. Such a finding has significant implications for endmember selection. Image-based endmember selection that identifies endmembers as the “purest” pixels may lead

to systematic bias in endmember fractions if the "purest" pixels are not spectrally representative of the endmembers. Such a bias can also occur in SMA using endmembers identified from the feature space. Endmembers not only need to be pure, but also to be representative. Representative endmembers may not necessarily be the most commonly seen endmembers. Analyses in this paper show that using the modes of the endmember signature distributions can lead to serious bias in endmember fractions if the endmember signature distributions are skewed. This finding also implies that care must be taken when collecting reference endmembers on the ground. Collecting reference endmembers requires a careful sampling design to ensure that the endmember signatures collected are spectrally representative of the endmembers.

This study used NDVI extensively in SMA to derive subpixel vegetation fractions. Several studies have shown that given the same amount of vegetation cover, the background conditions significantly influence the NDVI values (Elvidge & Lyon, 1985; Huete et al., 1985). Due to the nonlinear interaction between vegetation canopy and the background, particularly for photons in the near-infrared spectrum, we may overestimate vegetation fractions for very dark surfaces, and underestimate them with very bright backgrounds (Huete et al., 1985). In order to reduce the influence of soils on NDVI values, Huete (1988) developed the Soil Adjusted Vegetation Index (SAVI). Though such nonlinear interaction does not exist in simulated images, it does exist in real images. Results from tests using SAVI (results not shown) on the Ikonos image are nearly identical to those from NDVI, so soil background impacts do not appear to have been a problem in this study. This is perhaps because the sum of the reflectance values in the red and near-infrared spectra are approximately equal for vegetation and nonvegetation in the Ikonos image (Song, 2004). NDVI is linearly related to subpixel vegetation fractions under such a condition (Jasinski, 1990). Huete et al. (1985) found that NDVI is most sensitive to background conditions with intermediate vegetation cover (about 60 percent). In other words, the same intermediate vegetation cover can have very different NDVI values over different background conditions. The impact of soil background on NDVI in this study is quite different from that described by Elvidge and Lyon (1985) and Huete et al. (1985), where the nonlinear interaction happens vertically through the canopy. In this study, the emphasis is the horizontal mixture of endmembers. To a certain extent, BSMA can take into account the nonlinear interaction effect, as different NDVI values for the same vegetation cover over different backgrounds can be considered as signature variations.

6. Conclusions

This paper developed Bayesian Spectral Mixture Analysis (BSMA) to estimate subpixel vegetation fractions in the urban environment. The new approach explicitly accounts for the endmember variations in estimating subpixel vegetation fractions. In contrast to the traditional SMA, in which the spectral signatures of endmembers are treated as constants, BSMA uses the entire endmember signature distributions for SMA based on Bayes Theorem. A BSMA with two endmembers was first developed and then expanded to incorporate three endmembers. The model was tested with simulated and real remotely sensed data. When the endmember distributions are skewed, using the modes of endmember signature distributions as the endmembers leads to biased subpixel endmember fractions. BSMA produces significantly improved subpixel vegetation fractions compared to using the modes of the distributions. SMA using the means of endmember signature distributions generates subpixel endmember fractions with almost identical, and sometimes even greater accuracy, than those from BSMA. Such a finding has significant implications for endmember selection. Traditional endmember selection from the purest pixels or extremes in the feature space may lead to significant bias of subpixel endmember fractions if such selections differ from the means of the endmember signatures. An additional advantage of BSMA is that it provides uncertainty information for the estimated subpixel endmember fractions.

Acknowledgment

This research was supported in part by the Andrew W. Mellon Foundation under Grant 02081908 and in part by the National Science Foundation under Grant 0351430. The Author thanks Phil McDaniel and Yang Shao for help with image preparation, Daniel Weiss and Christine Erlien for help with manuscript preparation, and Dr. Feng Gao for help with programming. The author is in debt to the anonymous reviewers whose comments helped improve the quality of the paper significantly.

References

Adams, J. B., Sabol, D. E., Kapos, V., Filho, R. A., Roberts, D. A., Smith, M. O., et al. (1995). Classification of multispectral images based on fractions of endmembers: Application to land-cover change in the Brazilian Amazon. *Remote Sensing of Environment*, *52*, 137–154.

Asner, G. P. (1998). Biophysical and biochemical sources of variability in canopy reflectance. *Remote Sensing of Environment*, *64*, 234–253.

Asner, G. P., & Heidebrecht, K. B. (2002). Spectral unmixing of vegetation, soil and dry carbon cover in arid regions: Comparing multispectral and hyperspectral observations. *International Journal of Remote Sensing*, *23*(19), 3939–3958.

Asner, G. P., Wessman, C. A., & Privette, J. L. (1997). Unmixing the directional reflectances of AVHRR sub-pixel landcovers. *IEEE Transactions on Geoscience and Remote Sensing*, *35*(4), 868–878.

Atkinson, P. M., Cutler, M. E. J., & Lewis, H. (1997). Mapping sub-pixel proportional land cover with AVHRR imagery. *International Journal of Remote Sensing*, *18*(4), 917–935.

Bateson, A., & Curtiss, B. (1996). A method for manual endmember selection and spectral unmixing. *Remote Sensing of Environment*, *55*, 229–243.

Bateson, C. A., Asner, G. P., & Wessman, C. A. (2000). Endmember bundles: A new approach to incorporating endmember variability into spectral mixture analysis. *IEEE Transactions on Geoscience and Remote Sensing*, *38*(2), 1083–1094.

Carlin, B. P., & Louis, T. A. (1996). *Bayes and empirical bayes methods for data analysis*. London, UK: Chapman and Hall.

Carpenter, G. A., Gopal, S., Macomber, S., Martens, S., Woodcock, C. E., & Franklin, J. (1999). A neural network method for efficient vegetation mapping. *Remote Sensing of Environment*, *70*(3), 326–338.

Dai, X., & Khorram, S. (1998). The effects of image misregistration on the accuracy of remotely sensed change detection. *IEEE Transactions on Geoscience and Remote Sensing*, *36*(5), 1566–1577.

Defries, R. S., Hansen, M. C., & Townshend, J. R. G. (2000). Global continuous fields of vegetation characteristics: A linear mixture model applied to multi-year 8 km AVHRR data. *International Journal of Remote Sensing*, *21*(6-7), 1389–1414.

Drake, A. W. (1967). *Fundamentals of applied probability theory*. New York, NY: McGraw-Hill.

Elmore, A. J., Mustard, J. F., Manning, S. J., & Lobell, D. B. (2000). Quantifying vegetation change in semiarid environments: Precision and accuracy of spectral mixture analysis and the normalized difference vegetation index. *Remote Sensing of Environment*, *73*, 87–102.

Elvidge, C. D., & Lyon, R. J. P. (1985). Influence of rock–soil spectral variation on the assessment of green biomass. *Remote Sensing of Environment*, *17*, 265–279.

Garcia-Haro, F. J., Gilabert, M. A., & Melia, J. (1996). Linear spectral mixture modelling to estimate vegetation amount from optical spectral data. *International Journal of Remote Sensing*, *17*(17), 3373–3400.

Gong, P., & Zhang, A. (1999). Noise effect on linear spectral unmixing. *Geographic Information Sciences*, *5*(1), 52–57.

Hanan, N. P., Prince, S. D., & Hiernaux, P. H. Y. (1991). Spectral modelling of multicomponent landscapes in the Sahel. *International Journal of Remote Sensing*, *12*(6), 1243–1258.

Huete, A. R. (1988). A Soil Adjusted Vegetation Index (SAVI). *Remote Sensing of Environment*, *25*, 295–309.

Huete, A. R., Jackson, R. D., & Post, D. F. (1985). Spectral response of a plant canopy with different soil backgrounds. *Remote Sensing of Environment*, *17*, 37–53.

Hung, M., & Ridd, M. K. (2002). A subpixel classifier for urban land-cover mapping based on a maximum-likelihood approach and expert system rules. *Photogrammetric Engineering and Remote Sensing*, *68*(11), 1173–1180.

Jasinski, M. F. (1990). Sensitivity of the normalized difference vegetation index to subpixel canoy cover, soil albedo, and pixel scale. *Remote Sensing of Environment*, *32*(2-3), 169–187.

Ju, J., Kolaczyk, E. D., & Gopal, S. (2003). Gaussian mixture discriminant analysis and sub-pixel land cover characterization in remote sensing. *Remote Sensing of Environment*, *84*, 550–560.

Kerdiles, H., & Grondona, M. O. (1995). NOAA-AVHRR NDVI decomposition and subpixel classification using linear mixing in the Argentinean Pampa. *International Journal of Remote Sensing*, *16*(7), 1303–1325.

Madhavan, B. B., Kubo, S., Kurisaki, N., & Sivakumar, T. V. L. N. (2001). Appraising the anatomy and spatial growth of the Bangkok metropolitan area using a vegetation-impervious-soil model through remote sensing. *International Journal of Remote Sensing*, *22*(5), 789–806.

Mustard, J. F. (1993). Relationships of soil, grass, and bedrock over the Kaweah Serpentinite Melange through spectral mixture analysis of AVIRIS data. *Remote Sensing of Environment*, *44*, 293–308.

Okin, G. S., Roberts, D. A., Murray, B., & Okin, W. J. (2001). Practical limits on hyperspectral vegetation discrimination in arid and semiarid environments. *Remote Sensing of Environment*, *77*, 212–225.

Petrou, M., & Foschi, P. G. (1999). Confidence in linear spectral unmixing of single pixels. *IEEE Transactions on Geoscience and Remote Sensing*, *37*(1), 624–626.

Phinn, S., Stanford, M., Scarth, P., Murray, A. T., & Shyy, P. T. (2002). Monitoring the composition of urban environments based on the vegetation-impervious surface-soil (VIS) model by sub-pixel analysis techniques. *International Journal of Remote Sensing*, *23*(20), 4131–4153.

Qi, J., Marsett, R. C., Moran, M. S., Goodrich, D. C., Heilman, P., Kerr, Y. H., et al. (2000). Spatial and temporal dynamics of vegetation in the San Pedro River basin area. *Agricultural and Forest Meteorology*, *105*, 55–68.

Radeloff, V. C., Mladenoff, D. J., & Boyce, M. S. (1999). Detecting Jack Pine budworm defoliation using spectral mixture analysis: Separating effects from determinants. *Remote Sensing of Environment*, *69*, 156–169.

Ray, T. W., & Murray, B. C. (1996). Nonlinear spectral mixing in desert vegetation. *Remote Sensing of Environment*, *55*, 59–64.

Ridd, M. K. (1995). Exploring a V-I-S (vegetation-impervious surface-soil) model for urban ecosystem analysis through remote sensing: Comparative anatomy for cities. *International Journal of Remote Sensing*, *16*(12), 2165–2185.

Roberts, D. A., Gardner, M., Church, R., Ustin, S., Scheer, G., & Green, R. O. (1998). Mapping Chaparral in the Santa Monica Mountains using multiple endmember spectral mixture models. *Remote Sensing of Environment*, *65*, 267–279.

Roberts, D. A., Numata, I., Holmes, K., Batista, G., Krug, T., Monteiro, A., et al. (2002). Large area mapping of land-cover change in Rondonia using multitemporal spectral mixture analysis and decision tree classifiers. *Journal of Geophysical Research*, *107*(D20), 8073.

Roberts, D. A., Smith, M. O., & Adams, J. B. (1993). Green vegetation, nonphotosynthetic vegetation, and soils in AVIRIS data. *Remote Sensing of Environment*, *44*, 255–269.

Sabol, D. E., Adams Jr., J. B., & Smith, M. O. (1992). Quantitative subpixel spectral detection of targets in multispectral images. *Journal of Geophysical Research*, *97*(E2), 2659–2672.

Salvucci, G. D., & Song, C. (2000). Derived distribution of storm depth and frequency conditioned on monthly total precipitation: Adding value to historical and satellite-derived estimates of monthly precipitation. *Journal of Hydrometeorology*, *1*, 113–120.

Small, C. (2001). Estimation of urban vegetation abundance by spectral mixture analysis. *International Journal of Remote Sensing*, *22*(7), 1305–1334.

Small, C. (2003). High spatial resolution spectral mixture analysis of urban reflectance. *Remote Sensing of Environment*, *88*(1-2), 170–186.

Smith, M. O., Ustin, S. L., Adams, J. B., & Gillespie, A. R. (1990). Vegetation in Deserts: I. A regional measure of abundance from multispectral images. *Remote Sensing of Environment*, *31*, 1–26.

Song, C. (2004). Cross-sensor calibration between Ikonos and Landsat ETM+ for spectral mixture analysis. *IEEE Geoscience and Remote Sensing Letters*, *1*(4), 272–276.

Song, C., & Woodcock, C. E. (2003a). Monitoring forest succession with multitemporal Landsat images: Factors of uncertainty. *IEEE Transactions on Geoscience and Remote Sensing*, *41*(11), 2557–2567.

Song, C., & Woodcock, C. E. (2003b). Estimating tree crown size from multiresolution remotely sensed imagery. *Photogrammetric Engineering and Remote Sensing*, *69*(11), 1263–1270.

Souza, C., Firestone, L., Silva, L. M., & Roberts, D. (2003). Mapping forest degradation in the Eastern Amazon from SPOT 4 through spectral mixture models. *Remote Sensing of Environment*, *87*(4), 494–506.

Theseira, M. A., Thomas, G., Taylor, J. C., Gemmell, F., & Varjo, J. (2003). Sensitivity of mixture modeling to endmember selection. *International Journal of Remote Sensing*, *24*(7), 1559–1575.

Tompkins, S., Mustard, J. F., Pieters, C. M., & Forsytth, D. W. (1997). Optimization of endmembers for spectral mixture analysis. *Remote Sensing of Environment*, *59*, 472–489.

Townshend, J. R. G., Justice, C. O., Gurney, C., & McManus, J. (1992). The impact of misregistration on change detection. *IEEE Transactions on Geoscience and Remote Sensing*, *30*(5), 1054–1060.

Ward, D., Phinn, S. R., & Murray, A. T. (2000). Monitoring growth in rapidly urbanizing areas using remotely sensed data. *The Professional Geographer*, *52*(3), 371–386.

Wessman, C. A., Bateson, A., & Benning, T. L. (1997). Detecting fire and grazing patterns in tallgrass prairie using spectral mixture analysis. *Ecological Applications*, *7*(2), 493–511.

Wu, C., & Murray, A. T. (2003). Estimating impervious surface distribution by spectral mixture analysis. *Remote Sensing of Environment*, *84*, 493–505.

Yang, X., & Lo, C. P. (2002). Using a time series of satellite imagery to detect land use and land cover changes in the Atlanta, Georgia metropolitan area. *International Journal of Remote Sensing*, *23*(9), 1775–1798.